G. Van Eyndhoven, J. Sijbers, and K. J. Batenburg, "Combined Motion Estimation and Reconstruction in Tomography", 12th European Conference on Computer Vision, vol. 7583, Firenze, Italy, Lecture Notes on Computer Science, pp. 12-21, 2012.

Combined Motion Estimation and Reconstruction in Tomography

Geert Van Eyndhoven[1], Jan Sijbers[1], and Joost Batenburg[2]

[1] Vision Lab, University of Antwerp

[2] Centrum Wiskunde en Informatica, Science Park 123, NL-1098XG, Amsterdam, The Netherlands

Abstract. If objects or patients move during a CT scan, reconstructions suffer from severe motion artifacts. Time dependent computed tomography (4DCT) tries to minimize these artifacts by estimating motion and/or reconstruction simultaneously. Most current methods assume a known deformation or a reconstruction without artifacts at a certain time point. This work explores the possibilities of estimating the motion model and reconstruction simultaneously. It does so by modifying the simultaneous iterative reconstruction technique (SIRT) to incorporate motion (trans-SIRT) and uses this method in an optimization routine that computes motion and reconstruction at the same time. Results show that the optimization routine is able to estimate motion accurately, assuming only the type of parametrization for the motion model. Our approach can potentially be extended to more complex motion models.

Key words: Computed tomography, motion correction

1 Introduction

Time-dependent computed tomography (4DCT) is a highly active research area which involves the estimation of object and/or motion from tomographic projections acquired from an object subjected to some form of motion. Among its most obvious applications is the reconstruction of patient anatomy when scanning under free breathing conditions. Without compensation for motion, reconstructions suffer from serious motion artifacts. A standard technique to counter these motion artifacts is to minimize the motion itself by fixing the object or asking patients to hold their breath. There are, however, numerous situations where such precautions cannot be taken and hence other methods for 4DCT are being developed, which are roughly subdividable into two categories: gated CT and methods that explicitly incorporate a motion model.

Gated CT sorts projections into several phase bins and generates a reconstruction for every separate phase bin. The sorting can depend on an external breathing signal, which is currently acquired in most medical applications using external markers and a detection system [1], spirometry [2], or other data correlated to the breathing signal. Promising research has been reported where phase

bins are extracted from the tomographic data itself [3]. Since each phase bin reconstruction is created from only a fraction of all available projections, it lacks accuracy. In order to improve reconstruction quality, the correlation of reconstructions at adjacent phases can be exploited for temporal regularization [4, 5].
Another class of methods explicitly incorporates a motion model in the reconstruction algorithm, either in projection or object space. In projection space, the class of possible motion models for straight ray geometry is limited to affine transformations [6] and a slightly more general class, where the spacing and angles between rays can also be adapted [7]. If the condition of a straight ray geometry is relaxed, one can model any kind of deformation by properly adapting the projection matrix [8].
If the modeling is performed in object space, any transformation can be directly applied to the object. Usually, either the deformation or a motionless reconstruction is assumed to be known in advance. If the deformation is known, a modified Feldkamp or FBP algorithm can directly calculate a motionless reconstruction at a reference phase [9]. If a motionless reconstruction is assumed, the deformation can be estimated by a parameterized B-spline or PCA model that minimizes the projection distance [10, 11]. Several efforts have been made to generate general motion models. A popular modeling approach, which was already mentioned before, is the use of B-splines for parameterizing the motion field [10]. For modeling lung motion, Erthardt et al. created an 4D mean motion model using patient data, which can be adapted to a specific patient by performing a diffeomorphic image registration of a 3D volume at a reference phase to an average lung atlas [12]. By generating a patient specific lung motion model using PCA, a surrogate signal obtained from one marker could be sufficient to obtain the entire lung motion at a specific time point [13].
The above mentioned methods assume some kind of prior information. Gated CT assumes a motionless object for the duration of the scan in each phase bin, projection space modeling includes only a limited class of transformations, and object space modeling assumes a reference scan or a known deformation.
This paper describes a proof-of-concept study where as little prior information as possible is assumed. In Section 2, we start by introducing some notations and concepts and work our way forward to an iterative algorithm that reconstructs an object with given motion (trans-SIRT), which is thereafter used in an iterative optimization routine for estimating motion and object simultaneously. Simulation experiments and their corresponding results are discussed in Section 3 and 4. Finally, conclusions are drawn in Section 5.

2 Methods

2.1 Notations and Concepts

A 2D object can be described as a function $f : \mathbb{R} \times \mathbb{R} \to \mathbb{R}$. The projection process in tomography consists of straight rays traversing the object f at a certain angle θ and a signed distance s from the center of the detector to the ray (see Fig. 1). In a parallel beam geometry setup, the object is scanned at n_θ

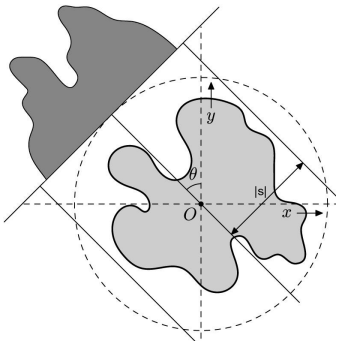

Fig. 1. Schematic overview of the projection process

angles, with all rays parallel per projection angle. In this paper, we use a parallel beam geometry with equidistant spacing between adjacent rays. To model the projection process, we introduce the 2D Radon transform

$$\mathcal{R}f(\theta, s) = \int_{-\infty}^{\infty} f\big((t\sin\theta + s\cos\theta), (-t\cos\theta + s\sin\theta)\big)\, dt \tag{1}$$

in which $\theta \in [0, \pi)$. The function $\mathcal{R}f(\theta, s)$ yields the integral of f along the line described by $x\cos\theta + y\sin\theta = s$ (Fig. 1). In a real tomographic scanner, there are only a finite number of detector pixels at a finite number of angles, denoted by d and n_θ, respectively. The (log-corrected) measured projection data $p_{\theta,s}$ at angle $\theta \in \{\theta_1, \ldots, \theta_{n_\theta}\}$ and offset $s \in \{s_1, \ldots, s_d\}$ can be ordered in a vector

$$\boldsymbol{p} = (p_{\theta_1,s_1}, \ldots, p_{\theta_1,s_d}, p_{\theta_2,s_1}, \ldots, p_{\theta_{n_\theta},s_d})^T \quad . \tag{2}$$

We refer to $\boldsymbol{p}$ as the *projection data* or the *sinogram*. The 2D object f can be approximated on a rectangular grid of N pixels, represented by a vector $\boldsymbol{x} = (x_1, \ldots, x_N) \in \mathbb{R}^N$, where we assume that f is constant over the domain of every pixel i. The line integral (1) can then be computed by the summation $\sum_{j=1}^{N} a_{ij}x_j$ where a_{ij} represents the contribution of pixel j to detector pixel i. Combining these discrete summations for all detector positions and all angles yields the system of linear equations $\boldsymbol{A}\boldsymbol{x} = \boldsymbol{p}$. Since this system is typically inconsistent, due to noise and discretization effects, one typically tries to minimize the projection distance $||\boldsymbol{A}\boldsymbol{x} - \boldsymbol{p}||$.

Now consider a time varying object $\{f_1, f_2, \ldots\}$, where f_i represents the object at time t_i. Throughout the paper, it will be assumed that motion during the acquisition of a single projection can be neglected and that the object can be represented on a pixel grid as $\{\boldsymbol{x}_1, \boldsymbol{x}_2, \ldots, \boldsymbol{x}_{n_\theta}\}$. Finally, we assume that at every time point t_i, the object is a transformation of the original object at time t_1: $\boldsymbol{x}_i = \boldsymbol{T}_{\theta_i}(\boldsymbol{x}_1)$ $(i = 1, \ldots, n_\theta)$. Evidently, this implies that $\boldsymbol{T}_{\theta_1}$ is the identity transformation. In practice, we calculate $\boldsymbol{T}_{\theta_i}(\boldsymbol{x}_1)$ by applying a deformation vector field (DVF) to the pixel coordinates of $\boldsymbol{x}_1$, followed by an interpolation

step to obtain the pixel values of $\boldsymbol{x}_i$. Since we use bilinear interpolation, we are able to represent $\boldsymbol{T}_{\theta_i}$ as an $N \times N$ matrix. Notice that this assumption does not restricts the object's motion to be linear, as this can be given by *any* DVF.

2.2 Trans-SIRT

In this section, the simultaneous iterative reconstruction technique (SIRT) [14] is modified to incorporate a known transformation. For every iteration k, the standard SIRT algorithm updates every jth pixel ($j = 1, \ldots, N$) as

$$x_j^{(k+1)} = x_j^{(k)} + \frac{\sum_i a_{ij} \left(p_i - \sum_h a_{ih} x_h^{(k)} \right) / \sum_h a_{ih}}{\sum_i a_{ij}} \quad . \tag{3}$$

Usually, $\boldsymbol{x}^{(0)}$ is taken to be a zero image. SIRT can also be represented in matrix notation as

$$\boldsymbol{x}^{(k+1)} = \boldsymbol{x}^{(k)} + \boldsymbol{C}\boldsymbol{A}^T\boldsymbol{R}(\boldsymbol{p} - \boldsymbol{A}\boldsymbol{x}^{(k)}) \quad , \tag{4}$$

where $\boldsymbol{C}$ and $\boldsymbol{R}$ are the diagonal matrices with inverse column and row sums, respectively. As is noted in [14], SIRT computes the solution of the weighted least square problem $\boldsymbol{x}^* = \operatorname{argmin}_{\boldsymbol{x}} \left(||\boldsymbol{A}\boldsymbol{x} - \boldsymbol{p}||^2_{\boldsymbol{R}} \right)$. To be able to introduce a known transformation in Eq. (4), we start by introducing some notations. Let $\boldsymbol{A}_{\theta_l}$ be the part of the projection matrix $\boldsymbol{A}$ that represents the projection in direction θ_l. Define

$$\tilde{\boldsymbol{A}} := \begin{bmatrix} \boldsymbol{A}_{\theta_1} & 0 & \cdots & 0 \\ 0 & \boldsymbol{A}_{\theta_2} & & 0 \\ \vdots & & \ddots & \vdots \\ 0 & 0 & \cdots & \boldsymbol{A}_{\theta_{n_\theta}} \end{bmatrix} \in \mathbb{R}^{dn_\theta \times n_\theta N}, \qquad \tilde{\boldsymbol{C}} := \begin{bmatrix} \boldsymbol{C} & 0 & \cdots & 0 \\ 0 & \boldsymbol{C} & & 0 \\ \vdots & & \ddots & \vdots \\ 0 & 0 & \cdots & \boldsymbol{C} \end{bmatrix} \in \mathbb{R}^{n_\theta N \times n_\theta N} \tag{5}$$

and

$$\boldsymbol{T} := \begin{bmatrix} \boldsymbol{T}_{\theta_1} \\ \vdots \\ \boldsymbol{T}_{\theta_{n_\theta}} \end{bmatrix} \in \mathbb{R}^{n_\theta N \times N}, \quad \boldsymbol{T}^{*-1} := \begin{bmatrix} \boldsymbol{T}_{\theta_1}^{-1} \cdots \boldsymbol{T}_{\theta_{n_\theta}}^{-1} \end{bmatrix} \in \mathbb{R}^{N \times n_\theta N} \quad . \tag{6}$$

The introduced notation allows us to describe the trans-SIRT algorithm as follows:

$$\boldsymbol{x}^{(k+1)} = \boldsymbol{x}^{(k)} + \boldsymbol{T}^{*-1}\tilde{\boldsymbol{C}}\tilde{\boldsymbol{A}}^T\boldsymbol{R}(\boldsymbol{p} - \tilde{\boldsymbol{A}}\boldsymbol{T}\boldsymbol{x}^{(k)}) \quad . \tag{7}$$

By an analogous argument as in [14], we will show the connection between trans-SIRT and the weighted least squares minimization problem

$$\operatorname*{argmin}_{\boldsymbol{y}} \left(||\tilde{\boldsymbol{A}}\boldsymbol{y} - \boldsymbol{p}||^2_{\boldsymbol{R}} \right) \quad \text{subjected to} \quad \boldsymbol{y} = \boldsymbol{T}\boldsymbol{x} \quad . \tag{8}$$

Multiplying the normal equations of Eq. (8) with $\boldsymbol{T}^{*-1}\tilde{\boldsymbol{C}}$ and replacing $\boldsymbol{y}$ with $\boldsymbol{T}\boldsymbol{x}$ gives

$$\boldsymbol{T}^{*-1}\tilde{\boldsymbol{C}}\tilde{\boldsymbol{A}}^T\boldsymbol{R}\tilde{\boldsymbol{A}}\boldsymbol{T}\boldsymbol{x} = \boldsymbol{T}^{*-1}\tilde{\boldsymbol{C}}\tilde{\boldsymbol{A}}^T\boldsymbol{R}\boldsymbol{p} \quad . \tag{9}$$

This can be rewritten as

$$(\boldsymbol{I} - (\boldsymbol{I} - \boldsymbol{T}^{*-1}\tilde{\boldsymbol{C}}\tilde{\boldsymbol{A}}^T\boldsymbol{R}\tilde{\boldsymbol{A}}\boldsymbol{T}))\boldsymbol{x} = \boldsymbol{T}^{*-1}\tilde{\boldsymbol{C}}\tilde{\boldsymbol{A}}^T\boldsymbol{R}\boldsymbol{p} \tag{10}$$

$$\Leftrightarrow \boldsymbol{x} = \boldsymbol{x} + \boldsymbol{T}^{*-1}\tilde{\boldsymbol{C}}\tilde{\boldsymbol{A}}^T\boldsymbol{R}(\boldsymbol{p} - \tilde{\boldsymbol{A}}\boldsymbol{T}\boldsymbol{x}) \quad . \tag{11}$$

Applying a fixed point iteration to Eq. (11) results in the iterative algorithm described by Eq. (7).
Note that we introduced Eq. (7) rather for the mathematical derivation and to have a compact description of trans-SIRT. In the implementation of trans-SIRT we calculate the transformation using bilinear interpolation and instead of multiplying with $\tilde{\boldsymbol{A}}$, the projections are calculated using $\boldsymbol{A}_\theta$ per projection angle θ. In Eq. (7), it was assumed that the inverse $\boldsymbol{T}_{\theta_i}^{-1}$ exists. This assumption is, however, not too restrictive, since realistic physical motion is invertible. Preferably an analytic inverse should be used. For more complex models this inverse will, however, no longer be available and must be calculated with a numerical method.

2.3 Simultaneous Estimation of Motion and Reconstruction

To simultaneously estimate object and motion, we use a motion model $\mathcal{T}$ depending on some parameters $\boldsymbol{\alpha}$[3], where we assume that the transformation $\boldsymbol{T}_\theta$ can be parameterized as $\mathcal{T}(\boldsymbol{\alpha}, \theta)$ for each angle θ. Discrete approximations of these transformations can be collected in a large matrix $\boldsymbol{T}(\boldsymbol{\alpha})$ analogous to Eq. (6). If we define $\boldsymbol{x}_1(\boldsymbol{\alpha})$ to be the trans-SIRT solution for motion model $\mathcal{T}(\boldsymbol{\alpha}, \theta)$, the optimal parameters $\boldsymbol{\alpha}$ (and hence also the optimal trans-SIRT solution $\boldsymbol{x}_1(\boldsymbol{\alpha})$) can be found by solving the following optimization problem:

$$\boldsymbol{\alpha}^* = \underset{\boldsymbol{\alpha}}{\operatorname{argmin}} \left(||\tilde{\boldsymbol{A}}\boldsymbol{T}(\boldsymbol{\alpha})\boldsymbol{x}_1(\boldsymbol{\alpha}) - \boldsymbol{p}||_2^2 \right) \quad . \tag{12}$$

Essentially, the solution of Eq. (12) minimizes the projection distance and hence optimizes the projections consistency. It does so by varying the motion model parameters $\boldsymbol{\alpha}$, computing an optimal trans-SIRT solution for these parameters and finally comparing the projections of this solution to the original projections. The function is minimized using the Levenberg-Marquardt algorithm (see for example [15]). Since the landscape of the objective function in Eq. (12) is rather coarse, the Jacobian needed by the Levenberg-Marquardt algorithm is computed using a finite difference scheme, starting from an initial stepsize which is halved every time the solver has found a minimum for the current stepsize.

3 Experiments

3.1 Trans-SIRT

To validate the trans-SIRT algorithm, a standard Shepp-Logan phantom of size 500×500 pixels was used, whereas the reconstruction was computed on a coarser

[3] Here, any motion model which transforms the pixel coordinates followed by an interpolation step can be used. A specific model will be tested in Section 3.

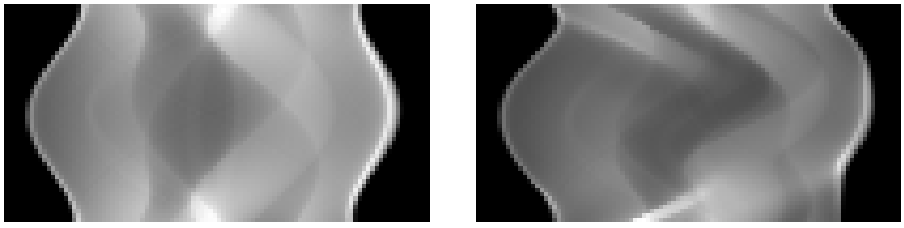

(a) Sinogram of Shepp-Logan without motion

(b) Sinogram of Shepp-Logan when B-spline based DVF is applied

Fig. 2. Sinogram of Shepp-Logan phantom

grid of 100×100 pixels. Projections are calculated from the phantom (500×500) using a strip kernel (see for example Section 7.4.1 of [16]). To compare trans-SIRT to regular SIRT, the following experiment was performed. A SIRT reconstruction was calculated using 51 projection angles uniformly sampled from the interval $[0, \pi]$ and a detector consisting of 100 pixels. A trans-SIRT reconstruction was computed using the same projection data, but regarding it as coming from a stationary detector and a moving Shepp-Logan phantom that turns in the opposite direction. In both cases, a circular reconstruction domain was used. The two cases are illustrated in Fig. 3(a). As a measure for accuracy, the root mean square error (RMSE) between reconstruction and phantom was calculated.
In another test, we used the same phantom but a rather complicated transformation represented by a DVF and based on quadratic B-splines using 6 knots in every dimension. The inverse DVF was calculated using Chen's method [17]. Again 51 equiangular projections (with 100 detectors each) were taken. The sinogram is displayed in Fig. 2.

3.2 Motion Parameter Estimation

For our experiments, we used a simple motion model that scales the object differently at every time point. If s_i is the scaling parameter at time t_i, then $f_i(x, y) = f_1(s_i x, s_i y)$. Instead of modeling every s_i individually, we approximate the time varying scaling coefficient series $\{s_i\}_{i=1,\ldots,n_\theta}$ by a cubic spline model with 12 or 16 parameters. The first scaling coefficient s_1 is forced to be 1 such that $\boldsymbol{T}_{\theta_1} = \boldsymbol{I}$. If this model would be regarded as a simplification of a breathing motion, then it would not be confined to regular breathing, since the spline approximation can model a large class of continuous function over a certain time interval. In a first test, the time varying scaling parameter series was the one displayed in Fig. 4(d). A spline model was used based on 12 parameters and uniform knot spacing. As a second test a more irregular scaling signal was employed, see Fig. 5(a). In this test, a spline approximation of 16 parameters and uniform knot spacing was used. The RMSE error was calculated for the

Table 1. aRMSE for each experiment and reconstruction

Experiment	True transformation	Gold standard	Optimized transformation
Regular signal	0.090319	0.1001	0.10156
Irregular signal	0.089871	0.10093	0.10302

reconstruction at every time point t_i and averaged to produce an average RMSE (aRMSE). The series $\{s_i\}_{i=1,\dots,n_\theta}$ was approximated directly by a cubic spline, which we then regarded as the gold standard. The same phantom was used as in the trans-SIRT validation. To make the experiment more realistic, Poisson distributed projections with incident beam intensity $I_0 = 50000$ (photon count) were generated from the simulated projection data. We used 50 SIRT iterations and 50 trans-SIRT iterations in every experiment. This number of iterations was determined experimentally to have the lowest RMSE in terms of reconstruction quality, when estimating motion parameters any number of iterations ranging from 20-500 gave equally good results.

4 Results

4.1 Trans-SIRT

In Fig. 3(b), the RMSE for SIRT and trans-SIRT is displayed as a function of the iteration number. We can see that the curves are almost identical. The fact that there is a difference can be explained by the discrete nature of our algorithm and the different types of interpolation for the two cases. That being said, the two solutions should approach one another in terms of RMSE (calculated between the reconstruction of case 1 and the reconstruction of case 2) if the resolution in the reconstruction domain increases. This was tested and the result is displayed in Fig. 3(c). The results for the spline based DVF are displayed in Fig. 3(d).

4.2 Motion Parameter Estimation

The results for the test with the regular scaling coefficient signal are displayed in Fig. 4. In Fig. 4(a)-(c), the reconstruction at time $t = 0$ is shown for regular SIRT (no motion correction), the gold standard (i.e. based on prior knowledge of the transformation) and the optimization problem in Eq. (12), respectively. Fig. 4(d) shows the starting values, the true scaling parameters, the gold standard, and the solution of the optimization problem with regards to time. The RMSE for every time point of the optimized reconstruction is shown in Fig. 4(e). The same figure was generated for the test with the irregular scaling parameter signal (Fig. 5). The aRMSE for each of the reconstructions is summarized in Table 1. It can be noticed that the optimization method does not require the signal to be regular to produce good results. Visually there is hardly any difference between the gold standard solution and the optimized solution, which is confirmed numerically in Table 1.

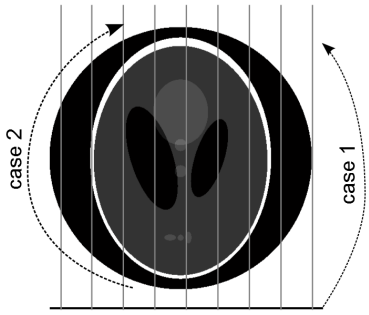

(a) Set up for experiment for case 1 and 2

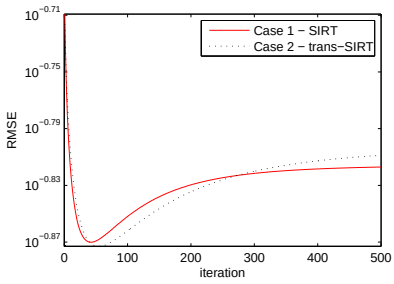

(b) RMSE of SIRT and trans-SIRT (case 1 and 2) as a function of iteration number

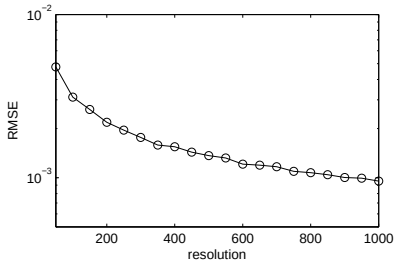

(c) RMSE between reconstruction in case 1 and reconstruction in case 2 as a function of resolution. Resolution grows from 50×50 with steps of 50 until 1000×1000

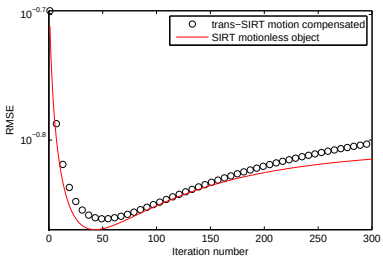

(d) RMSE as a function of iteration number for deformed Shepp-Logan phantom using spline based DVF

Fig. 3. A validation of trans-SIRT is performed in a first test (Fig. (a)-(c)), where a SIRT reconstruction is calculated using a rotating detector and a stationary object (case 1) and trans-SIRT is used to calculate a reconstruction for a stationary detector and rotating object (case 2). Figure (d) is the result of the experiment with the spline based DVF

5 Conclusion

We conducted a proof-of-concept in which motion and reconstruction is estimated simultaneously from tomographic data created with an object subjected to some form of motion. Simulation experiments confirmed the feasibility of this technique. For a known motion, trans-SIRT is able to produce results that are as accurate as regular SIRT for the same object without motion. We have also developed an optimization routine which simultaneously estimates motion and reconstruction, without the need for extra data. A major advantage of our approach is that any parameterized motion model can be incorporated and that only few assumptions were made, in contrast to many other current methods. A run of the optimization algorithm required about 5 minutes of computation

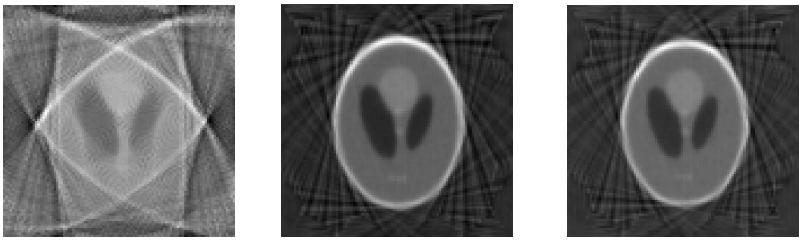

(a) Reconstruction without motion correction

(b) Gold standard reconstruction

(c) Reconstruction after optimization

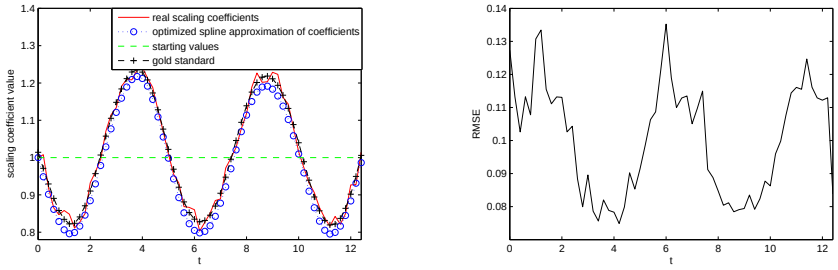

(d) Approximation of scaling parameters

(e) RMSE of optimized reconstruction

Fig. 4. Optimization results (regular scaling parameter signal)

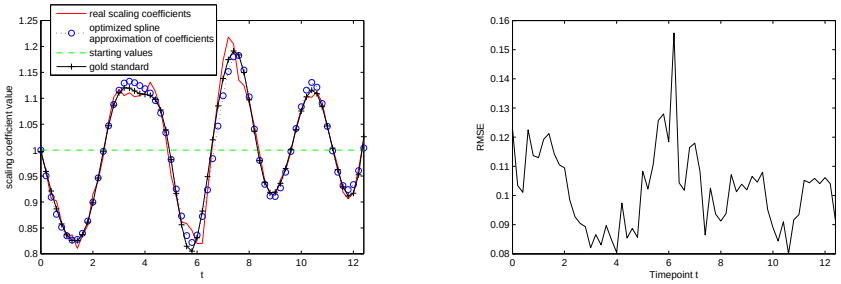

(a) Approximation of scaling parameters

(b) RMSE of optimized reconstruction

Fig. 5. Optimization results (irregular scaling parameter signal)

time when using an unoptimized GPU-based implementation of trans-SIRT. In future work we aim to extend our methodology to more complex motion models that have several parameters.

References

1. Vedam, S.S., Keall, P.J., Kini, V.R., Mostafavi, H., Shukla, H.P., Mohan, R.: Acquiring a four-dimensional computed tomography dataset using an external respiratory signal. Physics in Medicine and Biology **48** (2003) 45–62
2. Low, D.a., Nystrom, M., Kalinin, E., Parikh, P., Dempsey, J.F., Bradley, J.D., Mutic, S., Wahab, S.H., Islam, T., Christensen, G., Politte, D.G., Whiting, B.R.: A method for the reconstruction of four-dimensional synchronized CT scans acquired during free breathing. Medical Physics **30** (2003) 1254
3. Vergalasova, I., Cai, J., Yin, F.F.: A novel technique for markerless, self-sorted 4D-CBCT: Feasibility study. Medical Physics **39** (2012) 1442
4. Jia, X., Lou, Y., Dong, B., Tian, Z., Jiang, S.: 4D computed tomography reconstruction from few-projection data via temporal non-local regularization. Medical Image Computing and Computer Assisted Intervention (MICCAI) **13** (2010) 143–50
5. Gao, H., Cai, J.F., Shen, Z., Zhao, H.: Robust principal component analysis-based four-dimensional computed tomography. Physics in Medicine and Biology **56** (2011) 3181–98
6. Mooser, R., Forsberg, F., Hack, E., Székely, G., Sennhauser, U.: Estimation of affine transformations directly from tomographic projections in two and three dimensions. Machine Vision and Applications (October 2011) 1–16
7. Desbat, L., Roux, S.: Compensation of some time dependent deformations in tomography. IEEE Transactions on Medical Imaging **2** (2007) 1–20
8. Rit, S., Sarrut, D., Desbat, L.: Comparison of analytic and algebraic methods for motion-compensated cone-beam CT reconstruction of the thorax. IEEE Transactions on Medical Imaging **28** (2009) 1513–25
9. Li, T., Schreibmann, E., Yang, Y., Xing, L.: Motion correction for improved target localization with on-board cone-beam computed tomography. Physics in Medicine and Biology **51** (2006) 253–67
10. Docef, A., Murphy, M.J.: Reconstruction of 4D deformed CT for moving anatomy. International Journal of Computer Assisted Radiology and Surgery **3** (2008) 591–598
11. Staub, D., Docef, A., Brock, R.S., Vaman, C., Murphy, M.J.: 4D Cone-beam CT reconstruction using a motion model based on principal component analysis. Medical Physics **38** (2011) 6697–709
12. Ehrhardt, J., Werner, R., Schmidt-Richberg, A., Handels, H.: Statistical modeling of 4D respiratory lung motion using diffeomorphic image registration. IEEE Transactions on Medical Imaging **30** (2011) 251–65
13. Li, R., Lewis, J.H., Jia, X., Zhao, T., Liu, W., Wuenschel, S., Lamb, J., Yang, D., Low, D.a., Jiang, S.B.: On a PCA-based lung motion model. Physics in Medicine and Biology **56** (2011) 6009–30
14. Gregor, J., Benson, T.: Computational analysis and improvement of SIRT. IEEE Transactions on Medical Imaging **27** (2008) 918–24
15. Madsen, K., Nielsen, H.: Methods for non-linear least squares problems. Informatics and Mathematical Modelling - Technical University of Denmark (2004)
16. Kak, A.C., Slaney, M.: Principles of Computerized Tomographic Imaging. Society of Industrial and Applied Mathematics (2001)
17. Chen, M., Lu, W., Chen, Q., Ruchala, K.J., Olivera, G.H.: A simple fixed-point approach to invert a deformation field. Medical Physics **35** (2008) 81